Thermal Characterization of GaN-on-Diamond Substrates for HEMT Applications

Jungwan Cho[1], Zijian Li[1], Elah Bozorg-Grayeli[1], Takashi Kodama[1], Daniel Francis[2], Felix Ejeckam[2], Firooz Faili[2], Mehdi Asheghi[1], and Kenneth E. Goodson[1]
[1)] Department of Mechanical Engineering, Stanford University, Stanford, CA, 94305
[2)] Group4 Labs, Inc., Fremont, CA, 94539
Email: suksak82@stanford.edu

ABSTRACT

High-power operation of AlGaN/GaN high-electron-mobility transistors (HEMTs) requires efficient heat removal through the substrate. GaN composite substrates including high-thermal-conductivity diamond are promising, but high thermal resistances at the interfaces between the GaN and diamond can offset the benefit of a diamond substrate. We report on measurements of the thermal resistances at the GaN-diamond interfaces for two generations (1st and 2nd) of GaN-on-diamond substrates using a combination of picosecond time-domain thermoreflectance (TDTR) and nanosecond transient thermoreflectance (TTR) techniques. Two flipped-epitaxial samples are presented to determine the thermal resistances of the AlGaN/AlN transition layer. For the 2nd generation samples, electrical heating and thermometry in nanopatterned metal bridges confirms the TDTR results. This paper demonstrates that the latter generation samples, which reduce the AlGaN thickness by 75%, result in a strongly-reduced thermal resistance between the GaN and diamond. Further optimization of the GaN-diamond interfaces should provide an opportunity for improved cooling of HEMT devices.

KEY WORDS: High Electron Mobility Transistors (HEMT), Gallium nitride, Aluminum nitride, diamond, Thermal Boundary Resistance (TBR), thermal conductivity, Time-Domain Thermoreflectance (TDTR)

NOMENCLATURE

d	thickness (nm)
k	thermal conductivity (W m^{-1} K^{-1})
R	thermal resistance (10^{-9} m^2 K W^{-1})

Subscripts

ADH	adhesion film
Al	aluminum

I. INTRODUCTION

High-electron-mobility transistors (HEMTs) based on AlGaN/GaN are promising for high-power, high-frequency transistors and optoelectronic devices due to their high electron sheet charge densities and high electrical breakdown fields [1]. High-power operation exceeding 40 W/mm has been recently reported for a GaN-on-SiC configuration [2]. But localized device-level self-heating limits the peak power density and degrades device reliability [3]. The low thermal conductivity of the GaN buffer layer and the high thermal boundary resistances (TBRs) at interfaces in composite substrates impede efficient heat dissipation from the heated device region.

Integration of diamond films and composite diamond substrates within micrometers of active regions can be a compelling materials solution since polycrystalline diamond can have a thermal conductivity in the range 800-1800 W/m/K [4], which is much higher than those of SiC substrate (~400 W/mK) and sapphire (~35 W/mK). Recent efforts have used chemical-vapor-deposited (CVD) diamond substrates for AlGaN/GaN HEMTs [4]-[7]. The AlGaN/GaN epitaxial layers were first grown on a Si substrate by metal–organic chemical vapor deposition (MOCVD), and then atomically attached to CVD polycrystalline diamond [4]. Another study reported AlGaN/GaN heterostructures grown on (111) single crystal diamond substrate by molecular beam epitaxy (MBE) [8].

Thermal properties in diamond-based composite substrates have received much less attention. These composite substrates require careful attention to thermal resistances between the GaN and diamond, which can diminish the benefits of using the high conductivity material. Kuzmik *et al.* [9] used an optical transient interferometric mapping (TIM)technique to very approximately estimate the thermal resistance at the GaN-diamond interface for MBE-grown GaN on single crystalline diamond. These authors reported an upper bound (< 10 m^2K/GW) for the interface resistance. But these authors [9] provided no explanation for this relatively low TBR at the GaN-diamond interface, and the quality of their GaN buffer was not assessed. Also, their previous work [10] on a GaN-on-SiC substrate showed that their TIM approach has a large degree of uncertainty for extracting TBR (± 50%).

In this study, we extract the thermal resistances between the GaN and diamond for two types of GaN-on-diamond substrates (1st and 2nd generation) at room temperature using a combination of picosecond time-domain thermoreflectance (TDTR) and nanosecond transient thermoreflectance (TTR) techniques. Independent DC Joule heating measurements involving nanopatterned bridges confirm the TDTR results for the latter generation samples. We compare the thermal resistances at the GaN-diamond interfaces between the two generations, and show a progress in reducing the GaN-diamond thermal interface resistance.

II. SAMPLES AND EXPERIMENTAL METHODS

Fig. 1 illustrates the 1st and 2nd generation GaN-on-diamond substrates used in this study. The second generation targets a substantial reduction in thermal resistance by reducing the AlGaN transition layer thickness by approximately 75%. For both generations of samples, the

AlGaN/GaN heterostructure was grown on a Si substrate by metal-organic chemical vapor deposition (MOCVD). Following the MOCVD growth, this wafer was front-side mounted to a sacrificial carrier, and the Si substrate was etched away. The remaining AlGaN/GaN layers were attached to polycrystalline diamond using disordered adhesion layer of thickness (~50 nm) as described previously [4]. The 1st generation GaN-on-diamond substrate has a 1200 nm-thick transition layer consisting of 600 nm $Al_{0.5}Ga_{0.5}N$ and 600 nm AlN layer to reduce the effects of lattice mismatch between the substrate and the GaN buffer layer. The 2nd generation GaN-on-diamond substrates have a significantly reduced transition layer (142 nm $Al_{0.5}Ga_{0.5}N$ for sample A and 269 nm $Al_{0.5}Ga_{0.5}N$ for sample B). During the fabrication steps, the rest of the transition layer was etched away. Cross-sectional transmission electron microscopy (TEM) images confirm the sample dimensions for both types of samples.

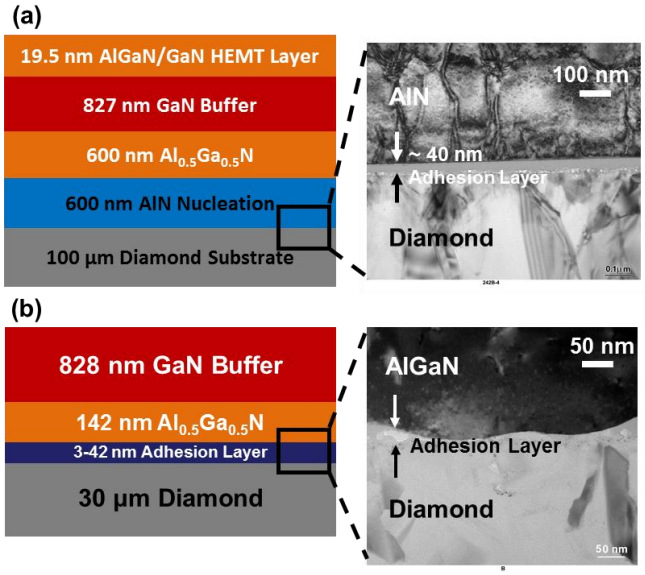

Fig. 1: Cross-sectional schematic drawings of the GaN-on-diamond substrates with representative cross-sectional TEMs near the adhesion layer: (a) 1st generation with a 1200 nm-thick $Al_{0.5}Ga_{0.5}N$/AlN transition layer and (b) 2nd generation with a significantly reduced transition layer.

Picosecond TDTR thermometry is well-established for determining near-surface thermal conductivities and interface resistances in multilayer thin film structures [11]-[14]. A passively mode-locked Nd:YVO4 laser with an 82 MHz repetition rate generates 9.2 ps pulses at wavelength λ=1064 nm. A beamsplitter separates these pulses into pump and probe components. The frequency-doubled pump beam, modulated by an electro-optic modulator (EOM) for lock-in detection, deposits heat in the metal transducer. The probe beam is temporally delayed from the pump via a linear delay stage, and the beam determines the reflectivity of the transducer film. For small temperature rises, the reflected intensity measures the surface temperature decay over 3.5 ns [15]. A 3-D radial symmetric heat diffusion solution for the multilayer stack is fitted to the normalized temperature decay to extract the properties of films beneath the metal transducer [11]. We validate system accuracy by extracting a thermal conductivity of 1.38 ± 0.05 W/mK for a SiO_2 calibration sample.

Nanosecond TTR thermometry uses longer timescales to investigate average transport properties within the material stack [16]. 6 ns pulses from a high power YAG laser heat the metal transducer, while another DC laser monitors the transient temperature rise at the surface for several microseconds after the pulse. An analytical heat transfer model assumes 1-D heat conduction since the pump beam waist is significantly larger than the thermal diffusion depth during the measurement.

DC Joule heating thermometry helps investigate and verify the thermal properties of the GaN-diamond interface. We fabricated gold nanoheaters with widths varying from 50nm to 5µm on top of the sample stack using the e-beam photolithography. The electrical thermometry captures the temperature by measuring the electrical resistance change in the nanoheaters. Different heater widths spatially confine the heat to a certain depth into the sample stack, yielding optimal sensitivity to different layers and interfaces. The temperature rise is measured by monitoring the voltage across the heater bridge. Since the temperature coefficient of resistivity (TCR) of Au is dependent on film thickness partly due to the electron scattering at film boundaries, a calibration is performed before each measurement. Data is fitted using a multilayer heat diffusion model to determine the thermal properties of the underlying material.

For the 1st generation GaN-on-diamond substrate, picosecond TDTR measurement is not sensitive enough to probe the resistance of the transition layer and the adhesion layer, since these layers are placed deep within the material stack. Thus, specialized samples were prepared using a flipped-epitaxy technique. For this sample geometry, the entire structure is flipped, with the flipped AlGaN/GaN heterostructure resting on a structure consisting of SiN_x and polysilicon (Fig. 2). Etching through the transition layer offers access to the $Al_{0.5}Ga_{0.5}N$ (Fig. 2a) and the AlN (Fig. 2b) through direct probing with picosecond TDTR. For the flipped AlN sample, the sample processing method left an additional 57 nm of SiN_x on the surface of the sample (Fig. 2b).

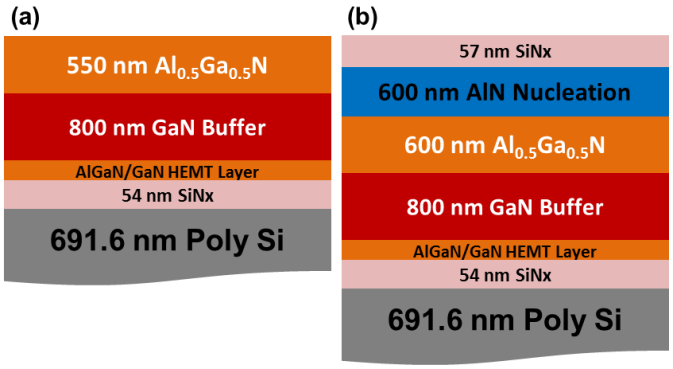

Fig. 2: Cross sectional schematic drawings of the flipped-epitaxial samples for (a) AlGaN transition layer and (b) AlN nucleation layer.

III. RESULTS AND DISCUSSION

A. 1st generation GaN-on-diamond substrate

For the 1st generation GaN-on-diamond substrate, the thermal resistances between the GaN and diamond ($R_{GaN\text{-}Diamond}$) consist of three components: the $Al_{0.5}Ga_{0.5}N$ intrinsic resistance (R_{AlGaN}), AlN intrinsic resistance (R_{AlN}), and the thermal resistance of the adhesion layer (R_{ADH}): $R_{GaN\text{-}diamond} = R_{AlGaN} + R_{AlN} + R_{ADH}$. The intrinsic resistances of the AlGaN and the AlN are determined by measuring two flipped-epitaxial samples with picosecond TDTR. Evaporated Al layers of 52 nm and 52.6 nm serve as the transducer for picosecond TDTR measurements on the flipped AlGaN and AlN samples, respectively. We use nanosecond TTR to measure the thermal resistance of the adhesion layer of the 1st generation GaN-on-diamond substrate coated with 150 nm Cr/100 nm Ti.

Fig. 3 shows a representative TEM image and the thermal trace with the best analytical fit for the flipped $Al_{0.5}Ga_{0.5}N$ sample. Data are fit assuming a semi-infinite behavior of the $Al_{0.5}Ga_{0.5}N$ transition layer since the thermal diffusion depth of 457 nm in the layer at 5 MHz pump modulation frequency is smaller than the layer thickness. The measurement is sensitive to the TBR between the Al transducer and $Al_{0.5}Ga_{0.5}N$ layer ($R_{Al\text{-}AlGaN}$), and to the thermal conductivity of the $Al_{0.5}Ga_{0.5}N$ layer (k_{AlGaN}). At room temperature, we find k_{AlGaN} = 16.6 ± 3.2 W/m/K and $R_{Al\text{-}AlGaN}$ = 21 ± 2.3 m^2K/GW. The error bars are due to uncertainty in the Al transducer thickness (d_{Al} = 52.0 ± 4.5 nm).

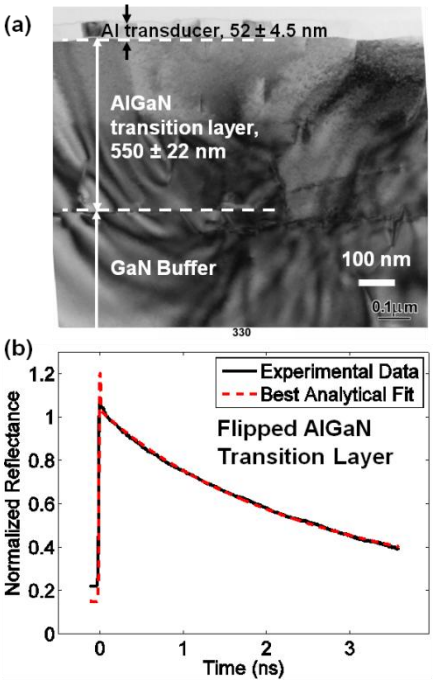

Fig. 3: (a) Representative cross-sectional TEM and (b) thermal trace with data fit for flipped AlGaN transition layer.

Daly *et al.* [17] used TDTR thermometry to extract $Al_xGa_{1-x}N$ thermal conductivity values that varied with the Al mass fraction (x) and temperature. At room temperature, these authors [17] found that the thermal conductivity of the polycrystalline $Al_{0.44}Ga_{0.56}N$ film grown by MOCVD on a sapphire substrate was around 6 W/mK, which is smaller than the measured thermal conductivity of the examined $Al_{0.5}Ga_{0.5}N$ film in this study. Liu *et al.* [18] did a similar study to measure the $Al_xGa_{1-x}N$ thermal conductivities using the 3ω method. They measured the thermal conductivity of the $Al_{0.4}Ga_{0.6}N$ film grown by hydride vapor-phase epitaxy (HVPE) on a c-plane sapphire substrate. Their measured room-temperature thermal conductivity was 25 W/mK, which is somewhat larger than the room temperature data in the present manuscript. The differences could be due to the crystalline quality of the AlGaN alloy, which depends on growth processes and growth substrates.

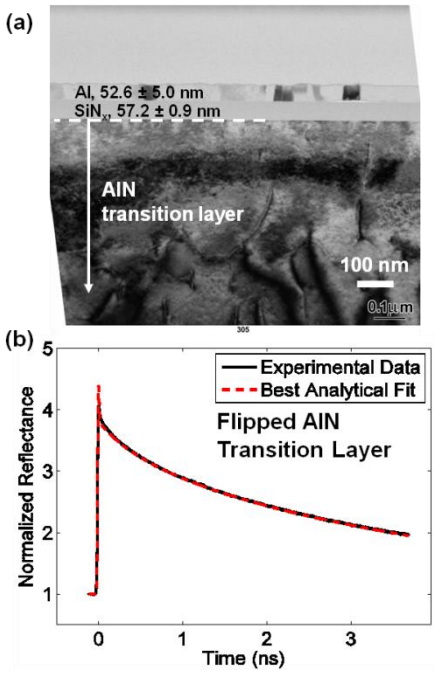

Fig. 4: (a) Representative cross-sectional TEM and (b) thermal trace with data fit for flipped AlN transition layer.

Figure 4 illustrates a representative cross-sectional TEM image and the thermal trace with the best analytical fit for the flipped AlN sample. The measurement is sensitive to the TBR between the Al transducer and SiN layer ($R_{Al\text{-}SiN}$), to the thermal conductivity of the SiN layer (k_{SiN}), and to the thermal conductivity of the AlN layer (k_{AlN}). Since the TBRs between the layers ($R_{SiN\text{-}AlN}$ and $R_{AlN\text{-}AlGaN}$) are convolved into k_{SiN} and k_{AlN}, we can extract only the effective thermal conductivity of each layer. At room temperature, we find $R_{Al\text{-}SiN}$ = 10.9 ± 0.6 m^2K/GW, k_{SiN} = 2.2 ± 0.4 W/mK, and k_{AlN} = 30.5 ± 5.0 W/mK. The error bars are due to variation in the thickness of the Al transducer (d_{Al} = 52.6 ± 5.0 nm). Manoi *et al.* [19] used micro Raman thermometry to investigate thermal conductivity values of MOCVD-grown AlN nucleation layers for GaN-on-SiC substrates. They found that the AlN thermal conductivities range between 1.5 and 23 W/mK at room temperature depending on crystalline quality and thickness of the AlN nucleation layer. A general trend of increasing AlN thermal conductivity with thickness was observed in their work, from an average of 2.2 W/mK for 40 nm-thick layers to 14.3 W/mK for 200 nm-thick layers. Their maximum AlN thermal

conductivity of 23 W/mK for a 200 nm-thick layer is comparable to our value of 30.5 W/mK, considering that the AlN has better crystalline quality with increasing layer thickness.

Nanosecond TTR measurement determines the room temperature thermal resistance of the adhesion layer (R_{ADH}) in the 1st generation GaN-on-diamond substrate. The measurement is sensitive to the effective thermal conductivity (k_{eff}) of the lumped stack, which includes a 20 nm HEMT layer, an 800 nm GaN buffer and a 1200 nm transition layer, and to the thermal resistance of the adhesion layer (R_{ADH}). The best analytical fit to the measured data yields an effective thermal conductivity of ~ 18.1 ± 6.5 W/mK. R_{ADH} is estimated to be 52 ± 15 m^{2}K/GW. The large uncertainties in R_{ADH} (~ 30%) are due to the following factors: (a) the complexity of the structure and oversimplification in thermal modeling, (b) spatial variations in thermal conductivity across various layers and (c) the presence of multiple interfaces.

B. 2nd generation GaN-on-diamond substrate

Picosecond TDTR measurements are performed on the two 2nd generation GaN-on-diamond substrates (Sample A and B) to extract the thermal resistances between the GaN and diamond. Table I summarizes sample dimensions, which were confirmed by cross-sectional TEM images. The thermal resistances between the GaN and diamond ($R_{GaN\text{-}Diamond}$) consist of two components: the $Al_{0.5}Ga_{0.5}N$ intrinsic resistance (R_{AlGaN}) and the thermal resistance of the adhesion layer (R_{ADH}): $R_{GaN\text{-}diamond} = R_{AlGaN} + R_{ADH}$. Here, the intrinsic resistance of the adhesion layer and the TBRs at its boundaries are lumped into a single resistance (R_{ADH}).

TABLE I. Geometries and thicknesses for the 2nd generation GaN-on-Diamond substrates

Sample	GaN thickness [nm]	$Al_{0.5}Ga_{0.5}N$ thickness [nm]	Adhesion layer thickness [nm]
A	828	142	3–42
B	848	269	38–55

The measurements aim at extracting the thermal resistances of the adhesion layer (R_{ADH}) in both samples. To accurately determine these values, all other thermal parameters must be known. The electrical thermometry determines the thermal conductivity of the GaN buffer layer. The narrow heaters (50 - 80nm) confine the heat within the top layers, so that the temperature rise in the heater is most sensitive to the thermal conductivity of the GaN. This measurement yields k_{GaN} = 90 W/mK. For the thermal conductivity of the $Al_{0.5}Ga_{0.5}N$ film, we utilize our measurement of the flipped sample (Section A). The diffuse mismatch model (DMM) [20], [21] predicts the GaN/AlGaN TBR to be 0.8 m^{2}K/GW. Small variations in the GaN/AlGaN TBR have little influence on the data extraction.

Table II summarizes all the measured values in both samples. Picosecond TDTR measurements determine that the thermal resistances of the adhesion layer range from 17 to 42 m^{2}K/GW. Further, we find the TBRs between the Al transducer and GaN buffer layer ($R_{Al\text{-}GaN}$) to be 10.6 ± 1.2 m^{2}K/GW for sample A and 10.2 ± 1.2 m^{2}K/GW for sample B. The uncertainty bars in these results are due to the effects of the Al transducer thickness (d_{Al} = 51.0 ± 3.5 nm). We perform DC Joule heating measurements on the same samples to verify the TDTR results. Wider heaters generate heat that penetrates deep into the layer stack and capture the adhesive thermal resistance. The measured thermal resistances at room temperature agree with the TDTR results within uncertainties.

TABLE II. Thermal resistance of adhesion layer for the 2nd generation GaN-on-Diamond substrates

Measurement technique	$R_{ADH,\,A}$ [m^{2}K/GW]	$R_{ADH,\,B}$ [m^{2}K/GW]
Picosecond TDTR	27 ± 10	31 ± 11
DC Joule heating	25 ± 11	29 ± 12

IV. SUMMARY AND CONCLUSION

The thermal resistances between the GaN and diamond ($R_{GaN\text{-}Diamond}$) are measured for both 1st and 2nd generation GaN-on-diamond substrates, using a combination of picosecond TDTR and nanosecond TTR techniques. Table III summarizes all the measurements for both 1st and 2nd generation samples. For the 1st generation samples, picosecond TDTR measurements on the two flipped-epitaxial samples determine the thermal conductivities of the AlGaN and AlN film (k_{AlGaN} and k_{AlN}). Nanosecond TTR measurement extracts the thermal resistance of the adhesion layer (R_{ADH}). For the 2nd generation samples, the thermal resistances of the adhesion layer (R_{ADH}) in two samples are extracted using picosecond TDTR. Independent DC Joule heating measurements on the same samples confirm the TDTR results. Utilizing k_{AlGaN} taken from the measurement on the flipped AlGaN sample, we determine the intrinsic resistance of the AlGaN layer.

TABLE III. Thermal resistances between GaN and diamond for both 1st and 2nd generation GaN-on-diamond substrates

	R_{AlGaN} [m^{2}K/GW]	R_{AlN} [m^{2}K/GW]	R_{ADH} [m^{2}K/GW]	$R_{GaN\text{-}diamond}$ [m^{2}K/GW]
1st gen	36 ± 8	20 ± 4	52 ± 15	108 ± 27
2nd gen, Sample A	9 ± 2	N/A	27 ± 10	36 ± 12
2nd gen, Sample B	16 ± 4	N/A	31 ± 11	47 ± 15

As Table III shows, the 2nd generation GaN-on-diamond substrates have significantly reduced GaN-diamond thermal interface resistances, which are less than half of that of the 1st generation samples. We can achieve a more reduced GaN-diamond thermal interface resistance by further etching the residual AlGaN layer. Recent simulation work has shown that the complete removal of the 1 µm transition layer reduces the temperature rise of the GaN-on-diamond configuration by up to 50% [22]. In the simulation, these authors have demonstrated that HEMT-on-diamond with a GaN-diamond thermal interface resistance of < 30 m^{2}K/GW can outperform HEMT-on-SiC even with zero GaN-SiC thermal interface resistance in terms of device temperature rise [22]. Therefore,

a further reduction in the GaN-diamond thermal interface resistance should be achieved and should eventually enhance cooling of HEMT-on-diamond devices.

ACKNOWLEDGMENTS

This work was supported by the DARPA Microsystems Technology Office (MTO) through Air Force contract FA8650-10-7044. J. Cho is supported by Samsung Scholarship, Z. Li is supported by Stanford Graduate Fellowship, and E. Bozorg-Grayeli is supported by National Defense Science and Engineering Graduate (NDSEG) Fellowship.

REFERENCES

[1] U. K. Mishra, P. Parikh, and Y. F. Wu, "AlGaN/GaN HEMTs-An Overview of Device Operation and Applications," Proceedings of the IEEE, vol. 90, no. 6, pp. 1022-1031, Jun. 2002

[2] Y. F. Wu, M. Moore, A. Saxler, T. Wisleder, and P. Parikh, "40-W/mm double field-plated GaN HEMTs," Proc. IEEE DRC Conf. Dig., p.151 , 2006.

[3] G. Meneghesso, G. Verzellesi, F. Danesin, F. Rampazzo, F. Zanon, A. Tazzoli, M. Meneghini, and E. Zanoni, "Reliability of GaN highelectron-mobility transistors: State of the art and perspectives," IEEE Trans. Device Mater. Rel., vol. 8, no. 2, pp. 332–343, Jun. 2008.

[4] D. Francis, F. Faili, D. Babic, F. Ejeckam, A. Nurmikko, H. Maris, "Formation and characterization of 4-inch GaN-on-diamond substrates", Diam. Rel. Mat., vol. 19, pp. 229-233, Feb. 2010.

[5] J. G. Felbinger, M. V. S. Chandra, Y. Sun, L. F. Lester, J. Wasserbauer, F. Faili, D. Babic, D. Francis, and F. Ejeckman, "Comparison of GaN HEMTs on diamond and SiC substrates," IEEE Electron Device Lett., vol. 28, no. 11, pp. 948–950, Nov. 2007.

[6] K. D. Chabak, J. K. Gillespie, V. Miller, A. Crespo, J. Roussos, M. Trejo, D. E. Walker, Jr., G. D. Via, G. H. Jessen, J. Wasserbauer, F. Faili, D. I. Babic, D. Francis, and F. Ejeckam, "Full-Wafer Characterization of AlGaN/GaN HEMTs on Free-Standing CVD Diamond Substrates." IEEE Electron Device Lett., vol. 31, no. 2, pp. 99-101, Feb. 2010.

[7] Q. Diduck, J. Felbinger, L. F. Eastman, D. Francis, J. Wasserbauer, F. Faili, D. I. Babic, and F. Ejeckam, "Frequency performance enhancement of AlGaN/GaN HEMTs on diamond," Electron. Lett., vol. 45, no. 14, pp. 758–759, Jul. 2009.

[8] M. Alomari, A. Dussaigne, D. Martin, N. Grandjean, C. Gaquiere, and E. Kohn, "AlGaN/GaN HEMT on (111) single crystalline diamond," Electron. Lett., vol. 46, no. 4, pp. 299–301, Feb. 2010

[9] J. Kuzmik, S. Bychikhin, D. Pogany, E. Pichonat, O. Lancry, C. Gaquiere, G. Tsiakatouras, G. Deligeorgis, and A. Georgakilas, "Thermal characterization of MBE-grown GaN/AlGaN/GaN device on single crystalline diamond," J. Appl. Phys., vol. 109, pp. 086106.1–086106.3, 2011.

[10] J. Kuzmik, S. Bychikhin, D. Pogany, C. Gaquiere, E. Pichonat, and E. Morvan, "Investigation of the thermal boundary resistance at the III-nitride/substrate interface using optical methods," J. Appl. Phys., vol. 101, no. 5, pp. 054 508.1–054 508.6, Mar. 2007.

[11] D. G. Cahill, "Analysis of heat flow in layered structures for time-domain thermoreflectance," Rev. Sci. Instrum., vol. 75, no. 12, pp. 5119–5122, Nov. 2004.

[12] M. A. Panzer, M. Shandalov, J. A. Rowlette, Y. Oshima, Y. W. Chen, P. C. McIntyre, and K. E. Goodson, "Thermal properties of ultra-thin hafnium oxide gate dielectric films," IEEE Electron Device Lett., vol. 30, no. 12, pp. 1269–1271, Dec. 2009.

[13] J. P. Reifenberg, K. W. Chang, M. Panzer, S. B. Kim, J. A. Rowlette, M. Asheghi, H. S. P. Wong, and K. E. Goodson, "Thermal Boundary Resistance Measurements for Phase-Change Memory Devices," IEEE Electron Device Letters, vol. 31, no. 1, pp. 56-58, Jan. 2010.

[14] J. Cho, E. Bozorg-Grayeli, D. H. Altman, M. Asheghi, and K. E. Goodson, "Low Thermal Resistances at GaN-SiC Interfaces for HEMT Technology", IEEE Electron Device Letters, in press.

[15] K. Ujihara, "Reflectivity of metals at high temperature," J. Appl. Phys., vol. 43, no. 5, pp. 2376–2383, May 1972..

[16] M. A. Panzer, G. Zhang, D. Mann, X. Hu, E. Pop, H. Dai, and K. E. Goodson, "Thermal properties of metal-coated vertically aligned single-wall nanotube arrays," J. Heat Transfer-Trans. ASME, vol. 130, pp.052401, May 2008.

[17] B. C. Daly, H. J. Maris, A. V. Nurmikko, M. Kuball, and J. Han, "Optical pump-and-probe measurement of the thermal conductivity of nitride thin films," J. Appl. Phys., vol. 92, no. 7, pp. 3820–3824, Oct. 2002.

[18] W. L. Liu and A. A. Balandin, "Thermal conduction in AlxGa1-xN alloys and thin films," J. Appl. Phys., vol. 97, no. 7, pp. 073710–073715, Apr. 2005.

[19] A. Manoi, J. W. Pomeroy, N. Killat, and M. Kuball, "Benchmarking of Thermal Boundary Resistance in AlGaN/GaN HEMTs on SiC Substrates: Implications of the Nucleation Layer Microstructure," IEEE Electron Device Lett., vol. 31, pp. 1395-1397, Dec. 2010.

[20] E. T. Swartz and R. O. Pohl, "Thermal boundary resistance," Rev. Mod. Phys., vol. 61, no. 3, pp. 605–668, Jul. 1989.

[21] L. De Bellis, P. E. Phelan, and R. S. Prasher, "Variations of acoustic and diffuse mismatch models in predicting thermal-boundary resistance," J. Thermophys. Heat Transf., vol. 14, no. 2, pp. 144–150, Apr.–Jun. 2000.

[22] Z. Li, M. Asheghi, and K. E. Goodson, "Impact of Composite Substrates on Near Junction Self Heating of High Electron Mobility Transistors," Electron. Lett., under review.